Biomechan Model Mechanobiol (2008) 7:227–242
DOI 10.1007/s10237-007-0087-9

ORIGINAL PAPER

The mechanobiological effects of periosteal surface loads

R. Dana Carpenter · Dennis R. Carter

Received: 15 November 2006 / Accepted: 4 April 2007 / Published online: 9 May 2007

Abstract We have developed an improved mechanobiological model of bone morphogenesis and functional adaptation that includes the influences of periosteum tension and pressure on bone formation and resorption. Previous models assumed that periosteal and endosteal bone deposition and resorption rates are governed only by the local intracortical daily stress or strain stimulus caused by cyclic loading. The new model incorporates experimental findings that pressures on periosteal surfaces can impede bone formation or induce bone resorption, whereas periosteal tensile strains perpendicular to bone surfaces can impede bone resorption or induce bone formation. We propose that these effects can produce flattened or concave bone surfaces in regions of periosteal pressure and bone ridges in regions of periosteal tension. The model was implemented with computer simulations to illustrate the role of adjacent muscles on the development of the triangular cross-sectional geometry of the rat tibia. The results suggest that intracortical stresses dictate bone size, whereas periosteal pressures may work in combination with intracortical stresses and other mechanobiological factors in the development of local bone cross-sectional shapes.

Keywords Bone · Mechanobiology · Biomechanics · Computational model · Periosteum

R. D. Carpenter · D. R. Carter
Bone and Joint Center,
Veterans Affairs Palo Alto Health Care System,
3801 Miranda Avenue, Palo Alto, CA 94304, USA

R. D. Carpenter · D. R. Carter
Biomechanical Engineering Group,
Mechanical Engineering Department, Stanford University,
Durand BME, Stanford, CA 94305, USA

Present address:
R. D. Carpenter (✉)
Musculoskeletal and Quantitative Imaging Research,
Department of Radiology, University of California,
1700 4th Street, Suite 203, San Francisco, CA 94158, USA
e-mail: dana.carpenter@radiology.ucsf.edu

1 Introduction

Although it is widely accepted that mechanical loading can affect skeletal morphology, it is unclear whether similarities and differences in bone cross-sectional structure can be used to make inferences about bone function. Georges Cuvier's concept of a "correlation of parts" proposed that anatomy reflects function and that the structure of each individual organ within an animal is related to those of all other organs (Rudwick 1997). In the context of skeletal mechanobiology, Cuvier's views are applicable to the effects of the mechanical environment on the processes of bone development and functional adaptation. In particular the structures directly adjacent to periosteal bone surfaces may affect bone cross-sectional morphology by modifying local bone modeling rates. Due to the effects of periosteal loads on bone morphology, anatomical and functional information about the structures surrounding bones may be necessary in order to fully understand the relationship between bone form and function.

Comparative anatomy can provide many insights into the relationships between different species. Consider, for example, the triangular cross-sectional morphology at the mid-diaphysis of the tibia. In mice, rats, cats, dogs, humans, and even elephants, the diaphysis of the tibia has a distinctly triangular shape, with flattened, slightly convex, or slightly concave periosteal surfaces at locations adjacent to the muscles of the lower leg (Sikes 1971; McClure et al. 1973;

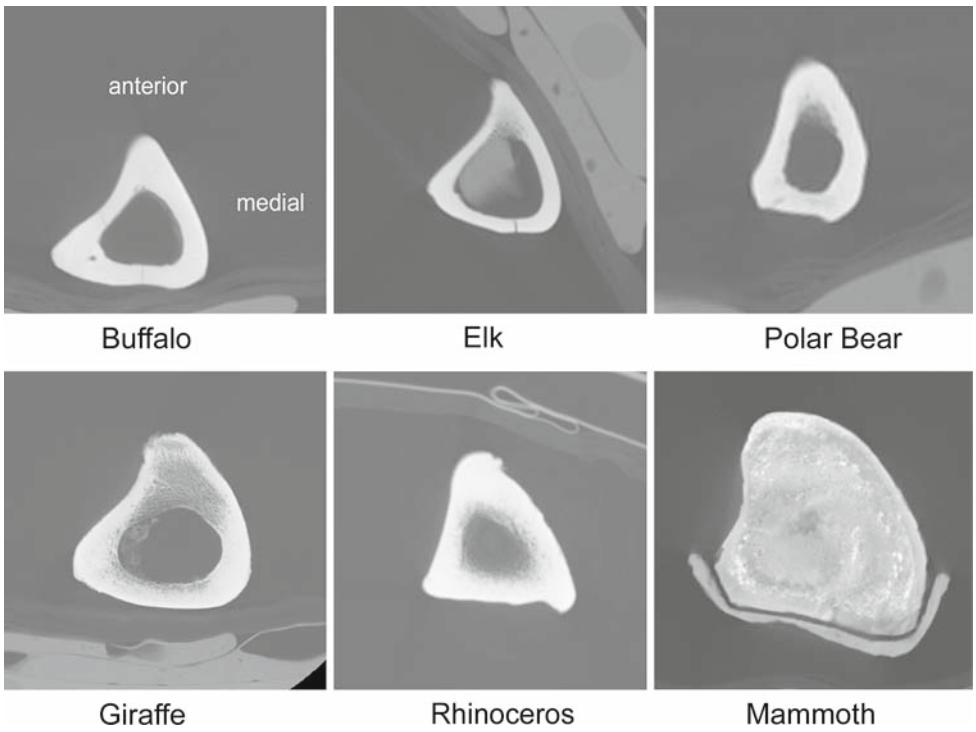

Fig. 1 Cross-sectional CT images of the *triangular diaphysis* of a buffalo, elk, polar bear, giraffe, rhinoceros, and mammoth tibia. Each image is oriented with the anterior/cranial and medial directions indicated on the buffalo image. Note that the mammoth image contains a plaster shell visible on the *posterior side*

Evans and Christensen 1979; Lanyon 1980; Martens et al. 1981). Many different extant and extinct species share this feature (Fig. 1). Given the large differences in size, anatomy, and biomechanics of locomotion that exist among a wide variety of animals, it may seem surprising that their tibiae all have similar cross-sectional shapes.

Previous studies have shown that normal muscle function during development is necessary in order to produce the normal triangular morphology of the tibial shaft in rats and in humans (Ráliš et al. 1976; Lanyon 1980). Therefore, the triangular shape of the tibia cannot be wholly attributed to genetic positional information. The relative anatomic locations of muscle bellies and overlying soft tissues adjacent to the tibial diaphysis may in fact produce a periosteal loading environment that is consistent among many terrestrial mammals, and the mechanobiological effects of this environment may be a crucial component of the process by which the triangular cross-sectional shape of the tibia develops (Fig. 2). This concept resonates with Lanyon's hypothesis of bone accommodation, which stated that bone morphology is often modified in order to accommodate adjacent structures (Lanyon 1980). Flattened bone surfaces often correspond to areas where muscle bellies contract and bulge out against the adjacent bone. The flattened lateral surface of the tibial shaft lies adjacent to the tibialis anterior muscle, which dorsiflexes the foot, and the flattened posterior surface of the tibial shaft lies adjacent to the soleus muscle, which produces plantar flexion. Conversely, raised crests or ridges appear at locations where muscles, ligaments, and membranes attach to bone surfaces. The anterior crest of the tibia and the interosseus crest on the lateral surface of the tibial shaft are two examples.

The surfaces of bones are surrounded by the cambium layer of the periosteum, which consists of multipotent cells that play a key role in bone morphogenesis and functional adaptation. The periosteal fibrous layer surrounds the cambium layer and lies adjacent to neighboring bones, muscles, blood vessels, tendons, ligaments, and skin. These surrounding structures can exert pressures and tensile strains on the periosteum in a direction perpendicular to the bone surface. Quasi-static, pulsatile, and intermittent surface pressures have been reported in the literature to lead to bone resorption or a decrease in bone formation in many different skeletal locations, including the vertebrae, ribs, phalanges, maxilla, middle ear, tibia, and cranial vault (Feik et al. 1987; Gooding et al. 1969; Hall and Watt 1986; King et al. 1991; Orisek and Chole 1987; Sato et al. 1998; Skripitz and Aspenberg 2000; von Böhl et al. 2004; Voyvodic et al. 1992; Wang and Hodges 1994). In contrast to the osteoclastic or reduced osteoblastic response to surface pressures, quasi-static tensile strains applied in a direction perpendicular to a bone surface due to bending of rat vertebrae, bending of early bone rudiments, brain growth, orthodontic force, periosteal distraction, and tumor growth have been shown to lead to bone apposition (Feik et al. 1987; Amprino 1985; Henderson et al. 2004; King et al. 1991; von Böhl et al. 2004; Schmidt et al. 2002; Yochum and Rowe 2005). Together, these studies suggest that, in addition to the intracortical stresses and strains arising due to axial, bending, and torsional loads applied

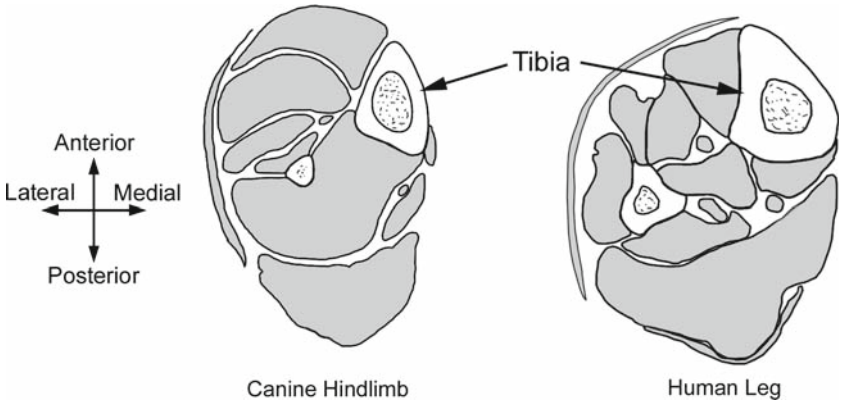

Fig. 2 Cross-sectional sketches of a canine hindlimb and a human leg. Muscles and other surrounding soft tissues are indicated by the *grey* zones. In both cases the tibia has a distinctly *triangular* shape, with dorsiflexor and toe extensor muscles adjacent to the lateral side and plantar flexor and toe flexor muscles adjacent to the posterior side. Canine sketch based on anatomical information from Evans and Christensen (1979); human sketch based on anatomical information from Agur and Lee (1991)

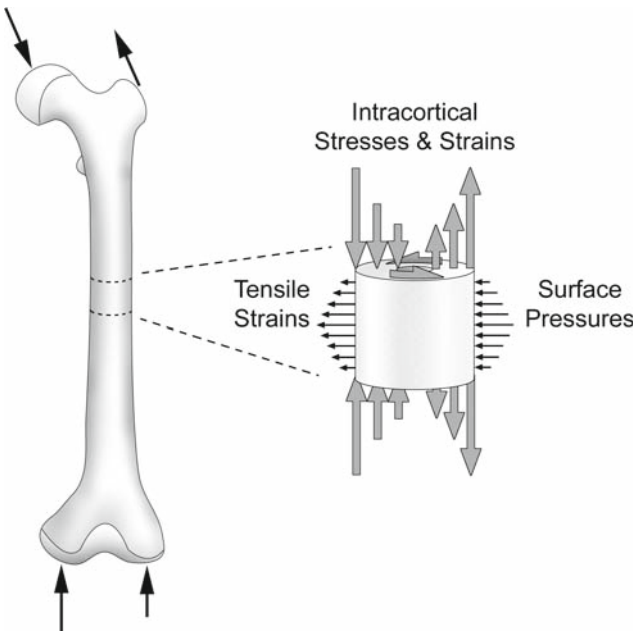

Fig. 3 The far-field loads applied to the femur shown on the *left* produce the intracortical stress distribution in the femoral shaft section illustrated on the *right*. Local loads applied directly onto the surface of the fibrous layer of the periosteum produce a distribution of periosteal surface pressures and normal tensile strains in the cell-rich cambium layer

relatively far from a given diaphyseal cross-section, bone modeling may also be affected by relatively small surface pressures and tensile strains applied in a direction perpendicular to the bone surface (Fig. 3).

In this paper we present a mechanobiological model that accounts for the effects of relatively small loads applied directly to periosteal surfaces of bones. This class of mechanical loads has previously been absent from mathematical models of bone development and adaptation. Our model, which is based upon experimental evidence obtained in a variety of animal and cell models, incorporates the findings that pressures applied directly to the periosteal surfaces of bones can impede bone formation or induce bone resorption. Conversely, tensile strains applied in a direction perpendicular to periosteal surfaces have been shown to impede bone resorption and, if high enough, induce bone formation. Computer simulations that implement this model help to explain how structures adjacent to bone diaphyseal surfaces affect bone cross-sectional morphology during development and throughout life.

2 Methods

2.1 Model development

The computational modeling framework presented below is built upon previous models that were used to simulate bone cross-sectional development and adaptation at the mid-diaphyses of long bones under the influence of axial, bending, and torsional loads applied relatively far from the cross-section of interest (Cowin 1984; Hart et al. 1984; Huiskes et al. 1987; van der Meulen et al. 1993; Levenston et al. 1998). These loads induce a distribution of intracortical stresses and strains throughout the section, and modeling rates corresponding to the local mechanical stimulus are determined using a modeling rate relationship. The same methods used in previous studies are presented here, but the modeling rate relationship has been modified in order to incorporate experimentally determined modeling rates (Fig. 4). The new model includes the effects of periosteal surface loads as described subsequently.

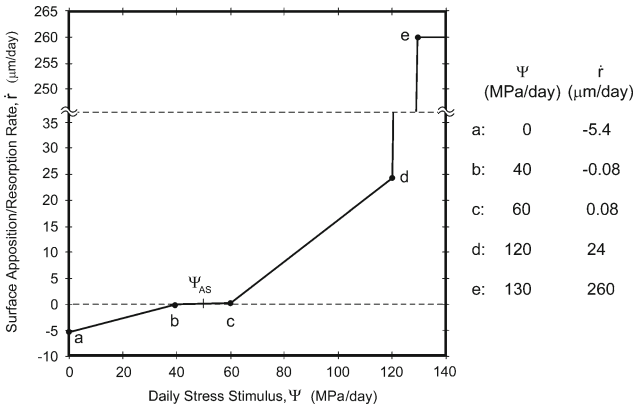

Fig. 4 Relationship between the daily stress stimulus (Ψ) and bone apposition or resorption rate ($\dot{r}$). *Positive values* of $\dot{r}$ indicate bone apposition, while *negative values* indicate bone resorption. The attractor state stimulus (Ψ_{AS}) is set at 50 MPa, and the *five lettered points* used to define the curve are listed to the *right*. References for these values are provided in the text

2.1.1 Intracortical stresses

A stress invariant called the energy effective stress ($\bar{\sigma}$), which is derived from the local strain energy density, can be used to summarize the stress state at any point within a bone (Fyhrie and Carter 1986). The energy stress does not differentiate between the tensile, compressive, and shear components of the stress tensor with respect to the local bone organization, but instead it provides a measure of the local magnitude of the strain energy stored at each point in the bone (Carter and Beaupré 2001). In the model the intracortical stress state at a point in a bone section with transversely isotropic material properties is summarized using $\bar{\sigma}$, which is computed using

$$\bar{\sigma} = \sqrt{\sigma_{zz}^2 + \left(\frac{E}{G}\right)\tau^2}\ \text{MPa}, \tag{1}$$

where σ_{zz} is the longitudinal normal stress, E is the elastic modulus of bone tissue in the longitudinal direction, G is the shear modulus of bone tissue for torsion about the shaft, and τ is the magnitude of the shear stress (Levenston et al. 1998). The surface modeling rate ($\dot{r}_p$ on the periosteal surface; $\dot{r}_e$ on the endosteal surface) is determined at each periosteal and endosteal location of a bone section based on the local value of the daily stress stimulus (Ψ), which is defined as

$$\Psi = \left(\sum_{\text{day}} n_i \bar{\sigma}_i^m\right)^{1/m}\ \text{MPa/day}, \tag{2}$$

where n_i is the number of daily cycles of load type i, $\bar{\sigma}_i$ is the tissue level effective stress due to load type i, and m is an empirical exponent (Carter et al. 1987; Beaupré et al. 1990a,b). The value of Ψ provides a measure of the cumulative modeling stimulus caused by intracortical stresses that the bone experiences in a given day. To obtain the local value of $\dot{r}_p$ or $\dot{r}_e$, the value of Ψ is compared to an attractor state stimulus (Ψ_{AS}), which is the optimal level of stimulus for bone maintenance. The local modeling error ($e = \Psi - \Psi_{AS}$) drives the bone modeling simulation. Alternatively, a daily strain stimulus can be computed based on applied cyclic strains (Mikic and Carter 1995). For simplicity the stress-based approach is used in the description of the modeling framework that follows.

The local values of $\dot{r}_p$ and $\dot{r}_e$ dictate whether bone tissue is to be added or removed at each surface location. These local surface apposition and resorption rates are determined using the relationship shown in Fig. 4. Following earlier studies, the attractor state stimulus Ψ_{AS} is set at 50 MPa/day, and a "lazy zone", in which bone is relatively insensitive to changes in loading, is set for a range of $100 \pm 20\%$ of Ψ_{AS} (Beaupré et al. 1990a,b; van der Meulen et al. 1993; Levenston et al. 1998). Based on a study of continued periosteal expansion of the adult femur, the modeling rates at the edges of the lazy zone (defined by points "b" and "c" in Fig. 3) are set at -0.08 μm/day for resorption and 0.08 μm/day for apposition (Ruff and Hayes 1982). The resorption rate for $\Psi = 0$ (point "a" in Fig. 3) is set at -5.4 μm/day, which was the maximum endosteal resorption rate that occurred in the immobilized forelimbs of old beagles (Jaworski et al. 1980; Cowin et al. 1985). Yielding (irreversible damage) begins to occur in cortical bone for stresses higher than 153 MPa in compression, 84 MPa in tension, and 56 MPa in shear (Jepsen and Davy 1997; Kaneko et al. 2003). To account for the rapid rate of bone apposition following the healing response to this damage, the rate of bone apposition is assumed to increase sharply for values of Ψ greater than 120 MPa/day. The modeling rate for $\Psi = 120$ MPa/day is set at 24 μm/day (point "d" in Fig. 3), which was the maximum rate of bone apposition reported during normal growth in rats (Sontag 1992). The maximum bone apposition rate for a healing response is set at 260 μm/day, which was the maximum rate reported in a study of distraction osteogenesis of the rat mandible (Loboa et al. 2004). The apposition rate is assumed to reach this level for a value of $\Psi = 130$ MPa/day (point "e" in Fig. 3), resulting in the sharp upward increase between 120 and 130 MPa/day.

2.1.2 Periosteal pressures and tensile strains

The local modeling rate determined using Fig. 4 is assumed to be induced by the intracortical stress within a bone's diaphyseal cortex. In addition to the effects of intracortical stress, our new model assumes that the bone modeling rate on the periosteal surface is then modified by pressures or tensile strains applied in a direction perpendicular to the periosteal surface. The effects of periosteal surface loads, which are described below, can be used to develop a mathematical model that takes into account the magnitude of the periosteal

surface pressure or tensile strain as well as the duration of load application.

Experimental results indicate that directly applied surface pressures of relatively small magnitude encourage osteoclast activity and differentiation in a load- and time-dependent manner. In an in vitro study, Kanzaki et al. (2002) applied direct pressures of approximately 0.05 and 0.28 kPa to cultured primary human PDL cells for a period of 6 or 24 h. After the load was removed, the PDL cells were cocultured with peripheral blood monocytes for a period of 4 weeks. Coculture with previously loaded PDL cells resulted in increased osteoclastic differentiation. Both higher load magnitude and load duration produced an increased amount of osteoclast differentiation, suggesting that applied pressure can affect ostoclastogenesis in both a load- and a time-dependent manner. In a study of intermittent and continuous pressure applied to the rat hard palate, an intermittent load of 19.6 kPa produced a significant increase in osteoclast activity, whereas a continuous load of only 6.86 kPa produced similar effects (Sato et al. 1998). Iwasaki et al. (2004) applied a range of orthodontic stresses ranging from 4 to 52 kPa and observed tooth migration in every case, and the velocity of tooth migration was higher for higher levels of applied stress. In order for a tooth to migrate through the jaw, bone must be resorbed in front of the tooth, where the PDL is under direct pressure. Therefore the rate of bone resorption was shown in this study to have a dose-dependent response to the magnitude of the applied orthodontic stress.

The periosteal response to directly applied pressure may consist of two types: a response to direct deformation due to small surface pressures and a response to impeded blood flow due to larger surface pressures. The study by Kanzaki et al. (2002) discussed above presents evidence for the effects of direct cellular deformation on osteoclastogenesis. In that study the direct deformation of PDL cells in culture resulted in an upregulation of receptor activator of nuclear factor κB ligand (RANKL), an essential factor for osteoclastogenesis. The results of the study showed that very small surface pressures may lead to osteoclastic differentiation in the PDL, and a similar response can be expected in the biologically similar periosteum.

Higher levels of applied surface pressure may interfere with normal blood flow and elicit a second type of mechanobiologic response. The range of stresses (4 to 52 kPa) applied in the Iwasaki et al. (2004) study of orthodontic tooth movement translates into a range of 30 to 390 mmHg. In a study of human skin blood perfusion, directly applied pressures of 11 to 50 mmHg were sufficient to stop blood flow (Ek et al. 1987). Pressures of a similar magnitude would likely have similar effects within the compliant tissue of the periosteum. The quasi-static stresses applied in the study of Iwasaki et al. would be sufficient to halt or at least interfere with the local blood supply. The bulging of the temporalis muscle during mastication in pigs has been shown to exert pressures ranging from 24.4 kPa (183 mmHg) to 122.7 kPa (920 mmHg) onto adjacent bone surfaces (Teng and Herring 1998). Although the pressures produced by muscle contractions are intermittent, they have the ability to affect the relatively constant capillary blood flow in the adjacent periosteum.

Impeded blood flow can lead to hypoxic or even anoxic conditions, and these conditions have been shown to promote bone resorption and inhibit osteogenesis. Hypoxic levels of 5 and 2% O_2 have been shown to lead to increased size and number of osteoclasts in cultures of osteoclast precursors from mice (Arnett et al. 2003). In this same study, hypoxic levels of 12, 5, and 2% O_2 led to 4-, 9-, and 21-fold increases, respectively, in bone resorption on ivory (dentine) wafers. The authors of this study state that some leakage of oxygen into the hypoxic cultures occurred during the 7-day culture period, indicating that even transient levels of hypoxia can lead to increases in osteoclast size, number, and activity. In addition to its effects on osteoclastogenesis, impeded blood flow may also affect osteoblast differentiation and activity. Anoxia (<0.02% O_2) for periods of 12 and 24 h has been shown to downregulate Runx2, a transcription factor necessary and sufficient for osteoblast differentiation, and to inhibit bone nodule formation in cultures of primary calvarial osteoblasts from mice and in the osteoblast-like immortalized MC3T3-E1 cell line (Salim et al. 2004).

The biological responses of bone cells and bone cell precursors to applied tensile strains have been explored in several experimental studies. When primary murine calvarial osteoblasts were subjected to a 10% static, equibiaxial tensile strain, proliferating cell nuclear antigen (a marker of cell proliferation) increased by three-fold after 24 h and six-fold after 48 h (Fong et al. 2003). In addition to the increase in osteoblast proliferation observed in this study, expression of FGF-2 and TGF-β1 (osteogenic growth factors), transcription of collagen I (the primary organic constituent of bone), and expression of VEGF (an angiogenic factor expressed by osteoblasts during bone growth) were all increased in osteoblast cultures subjected to static tensile strains. Similar results were found by Kanno et al. (2005) in cultures of human periosteal cells subjected to relatively slow (1/20 Hz) cyclic tensile strains of 12%. In this study FGF-2, TGF-β1, VEGF, and procollagen I (soluble precursor to collagen I) all increased as a result of applied tensile strains. In addition to tests performed on cells in culture, the ostegenic effects of tensile strain have also been shown in intact cranial sutures. Quasi-static tensile strains exerted by torsional springs were shown to increase production of BMP-4 (a bone morphogenic protein) and Cbfa1 (an osteoblast-specific transcription factor, also called Runx2) in the cranial sutures of mice in organ culture (Ikegame et al. 2001). The many similarities between cranial sutures, the PDL, and the periosteum suggest that the response of

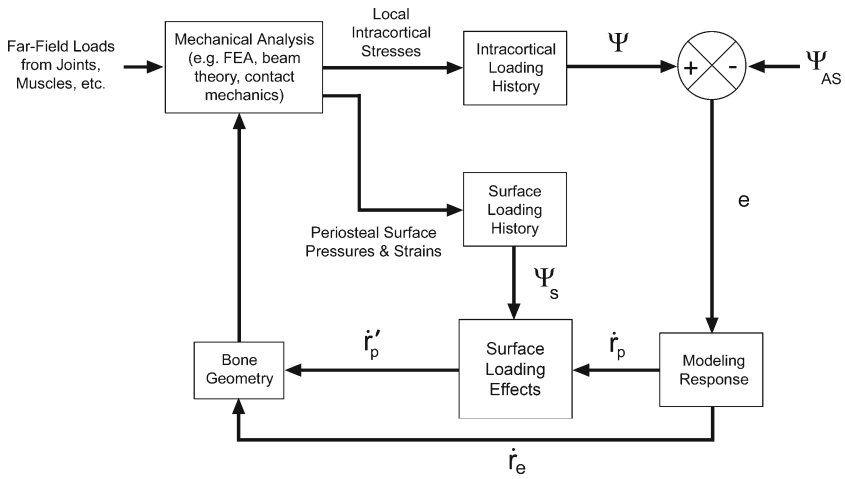

Fig. 5 Flow chart of bone modeling simulations accounting for both intracortical stresses and direct periosteal loads. The outer loop accounts for the effects of intracortical stresses, and the inner loop accounts for the effects of periosteal surface loads

these fibrous tissues to mechanical loads may be governed by the same general set of mechanobiological principles (Henderson and Carter 2002).

To quantify the effects of periosteal surface loads on bone modeling, a new simulation structure was developed (Fig. 5). Both the periosteal load magnitude and duration are included in the simulation to account for the load and time dependence observed in the studies discussed above. In the new model the magnitudes of the surface loads at a given periosteal location, when combined with information on the amount of time each load is applied in a given day, are used to compute the surface modeling stimulus, Ψ_s, using

$$\Psi_s = \frac{\sum_{\text{day}} \lambda_i t_i}{t_d} \text{ MPa/day (stress) or \%/day (strain)}, \quad (3)$$

where λ_i is the magnitude of the local surface pressure or tensile strain i, t_i is the total length of time during which λ_i is applied in a day, and t_d is the total amount of time in a day (e.g. 24 h or 86,400 s). For periosteal surface tensile strains, Ψ_s has a positive value. For periosteal surface pressures, Ψ_s has a negative value. For example, a static pressure of magnitude λ MPa that is applied throughout an entire day would yield $\Psi_s = -\lambda$ MPa/day. A cyclic tensile strain of magnitude λ% applied in 1-s increments 10,000 times per day would yield $\Psi_s = +0.116\lambda$ %/day. This time averaging method accounts for the more potent effects of continuously applied loads measured in the rat hard palate by Sato et al. (1998).

At endosteal locations the local value of $\dot{r}_e$ alone dictates whether bone tissue should be added or removed, and the geometry of the bone section is modified accordingly. However, at periosteal surface locations subject to periosteal surface pressures or tensile strains, linear interpolation between $\dot{r}_p$ and the maximum rate of bone resorption or apposition is used to determine the modeling rates corresponding to specific combinations of $\dot{r}_p$ and Ψ_s. The modified periosteal modeling rate $\dot{r}'_p$ is computed by interpolating between the modeling rate law in Fig. 4 and maximum modeling rates measured in experimental studies. The highest possible apposition rate due to surface tensile strain alone was set at 260 μm/day and was assumed to occur for an applied normal periosteal tensile strain of 10% (Loboa et al. 2004). In a study of human tooth migration (Iwasaki et al. 2004), the highest rate of orthodontic tooth movement was 85 μm/day. This rate was used as the maximum rate of bone resorption due to an applied periosteal surface pressure. Based on a no-intercept linear curve fit of the Iwasaki data, this resorption rate is assumed to occur for an applied periosteal surface pressure of −57.5 kPa. Because no capillary blood flow (and therefore no bone formation) occurs in soft tissues under an applied surface pressure of approximately −6.7 kPa or −50 mmHg (Ek et al. 1987), it is assumed that a transition from bone apposition to bone resorption occurs at this level of applied pressure regardless of the size of the intracortical modeling stimulus.

Periosteal loads in combination with intracortical stresses cause a shift in the modeling rate relationship (Figs. 6 and 7). The application of periosteal surface pressure flattens the curve and moves the curve toward the maximum rate of resorption. For a pressure-induced Ψ_s of −64 kPa/day or lower, the maximum resorption rate of −85 μm/day is induced. The application of normal periosteal tensile strains also flattens the curve, but in this case the curve moves toward the maximum rate of bone apposition. For a tension-induced Ψ_s of 10%/day or higher, the maximum apposition rate of 260 μm/day is induced.

To facilitate comparisons with studies of bone modeling that utilize strain gage measurements to quantify the intracortical strains instead of stresses, a set of curves can be created using the daily strain stimulus approach of Mikic and Carter (1995) (Fig. 7). This approach is analogous to the daily stress stimulus approach discussed previously, with the daily strain stimulus ξ computed as

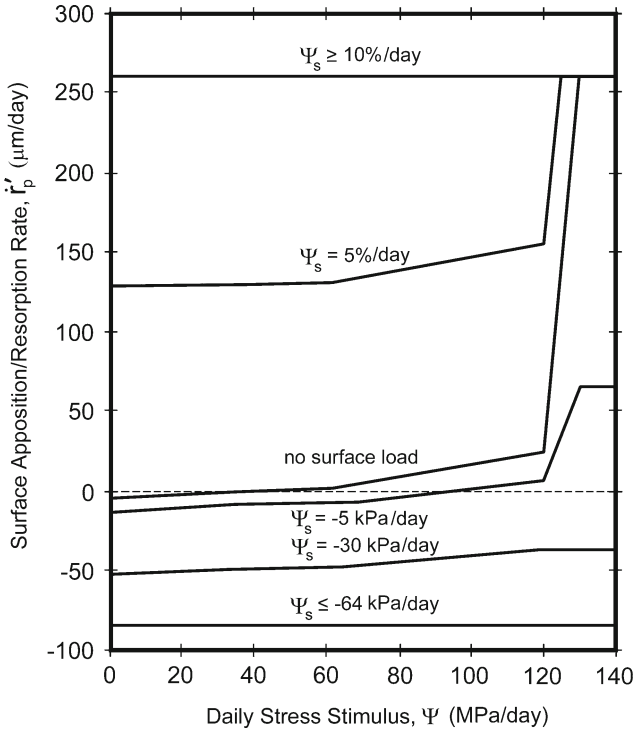

Fig. 6 Relationship between modified bone apposition rate, daily stress stimulus, and surface modeling stimulus (Ψ_s). *Positive modeling rate values* indicate bone apposition, while *negative values* indicate bone resorption. Note that *curves* representing the effects of periosteal surface pressures are labeled in units of kPa/day, while periosteal tensile strains are labeled in units of %/day

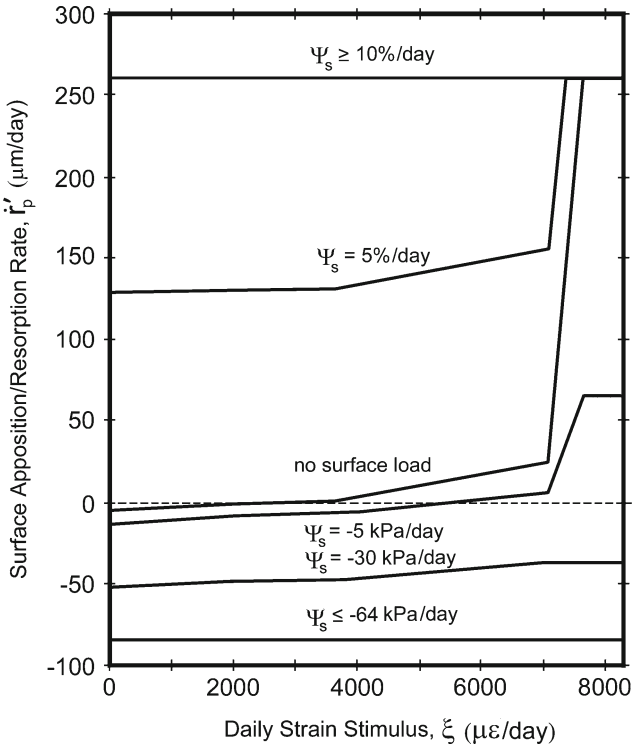

Fig. 7 Relationship between modified bone apposition rate, daily strain stimulus, and surface modeling stimulus (Ψ_s). *Positive modeling rate values* indicate bone apposition, while *negative values* indicate bone resorption. Note that *curves* representing the effects of periosteal surface pressures are labelled in units of kPa/day, while periosteal tensile strains are labelled in units of %/day

$$\xi = \left(\sum_{\text{day}} n_i \bar{\varepsilon}_i^m \right)^{1/m} \quad \mu\varepsilon/\text{day}, \tag{4}$$

where $\bar{\varepsilon}_i$ is the energy equivalent strain calculated as

$$\bar{\varepsilon}_i = \frac{\bar{\sigma}_i}{E_{11}}, \tag{5}$$

where E_{11} is the longitudinal elastic modulus of cortical bone. In the calculations used to produce Fig. 7, a value of 17 GPa was used for E_{11} (Reilly and Burstein 1975).

The theoretical framework developed here is the first to incorporate the mechanobiological effects of both intracortical stresses and local periosteal loads. The result is a more complete and realistic characterization of the influence of the mechanical environment on bone surface modeling rates. The curves provided in Figs. 6 and 7 provide a quantitative basis for exploring the effects of periosteal surface pressures and tensile strains on bone morphogenesis. One of the most evident features of the relationships is that relatively small surface loads appear to exert a powerful influence on local periosteal bone modeling rates. In order to determine the effects of these loads on bone cross-sectional structure, the modeling framework introduced in this section was used to drive iterative computational simulations of bone development. In the study described subsequently, this approach is used to examine the effects of periosteal loads on bone cross-sectional morphology during development of the tibia in rats.

2.2 Rat tibia simulation

In a study of tibial geometry in growing rats, Ráliš et al. (1976) found that severing the motor nerve to the dorsiflexors or plantiflexors caused the adjacent bone surface to develop a fully convex shape as opposed to the normally flattened or slightly convex shape. Similarly, Lanyon (1980) found that severing the sciatic nerve, which controls motor function in the hindlimbs of rats, caused the tibia to develop a distinctly round shape as opposed to the triangular shape seen in normal cases (Fig. 8). In addition to the striking difference in cross-sectional geometry that Lanyon observed, the neurectomized tibiae also had an 11% smaller width (statistically significant at $P < 0.01$) in the anterior–posterior direction as compared to that of the nonoperated limbs.

To recreate Lanyon's experimental results, the theoretical framework developed above was used to simulate the effects of periosteal surface pressures and intracortical stresses on

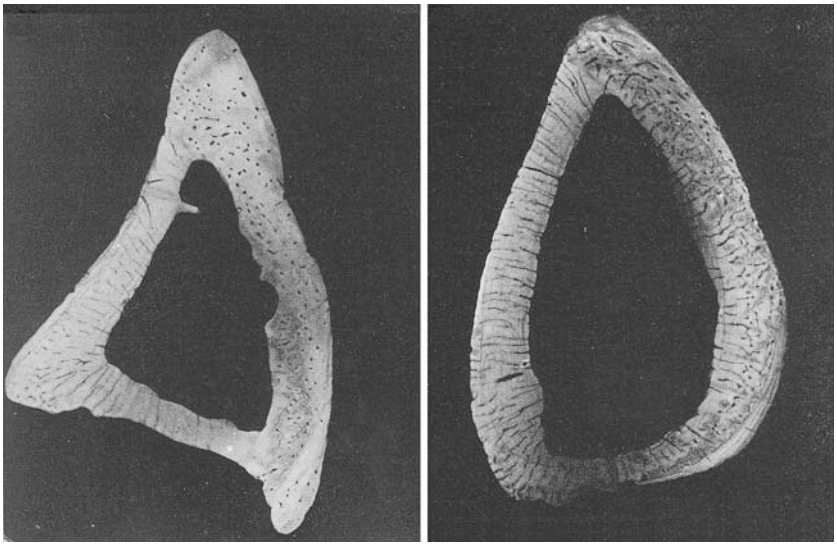

Fig. 8 17-month-old tibial cross-sections from a normally functioning rat hindlimb (*left*) and from the hindlimb of a rat that received a sciatic neurectomy at an age of 28 days (*right*). Adapted from Lanyon (1980)

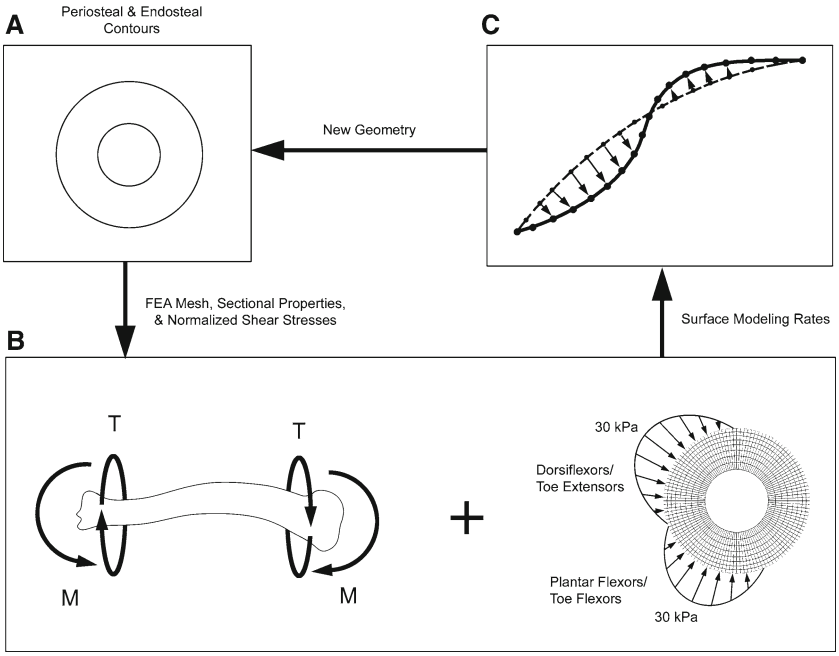

Fig. 9 Analysis steps of bone modeling simulations. **a** VA-Twist analyzed the inner and outer contours of a bone cross-section and produces a finite element mesh, a list of sectional properties, and a list of normalized torsional shear stresses for each node in the mesh. **b** The bone modeling program computes local surface modeling rates based on the intracortical stresses induced by far-field bending and torsional loads and the applied periosteal pressures exerted by the adjacent musculature. **c** Based on the local modeling rate, points on the contours are moved in a direction corresponding to the local surface normal. The *dashed line* indicates a segment of the original contour, and the *solid line* indicates a segment of the new, modified contour. The modified periosteal and endosteal contours serve as the starting point for the next time step

the development of the tibia in rats. Lanyon's experiment included a group of control rats and a group of experimental rats that received a sciatic neurectomy at an age of 4 weeks. Both groups were then grown in cages for an additional 16 months. At the end of the experiment, the animals were killed and the microradiographs of the tibial cross-sections were obtained (Fig. 8). In the computational model described here, a tibia was "grown" to an age of 28 days, and then a "control" tibia and a set of "experimental" tibiae were grown for an additional 16 months using the 28-day-old geometry as a starting point. A description of the software used in the study, and the specific geometry and applied loads used in each simulation are presented in the sections that follow.

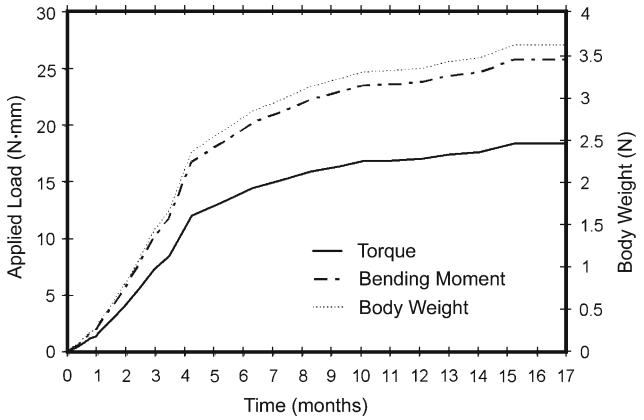

Fig. 10 Applied torque and bending moment magnitudes used in bone modeling simulations. The loads were scaled with body mass data from growing rats Donaldson 1924. Note that a time of 0 months corresponds to 6 days before birth

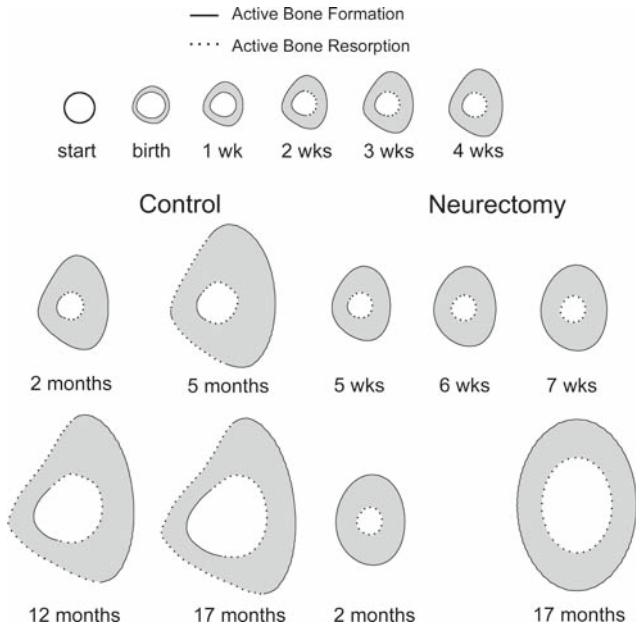

Fig. 11 Results of the control and full-load neurectomy simulations. The initial series at the *top* of the figure shows the results of the simulation from the start (6 days before birth) to an age of 4 weeks. Age since birth is listed *below* each bone section

2.2.1 *Computer software*

A custom computer program was written in the C programming language and used in conjunction with the public domain finite element software VA-Twist (Levenston et al. 1998) to perform the bone modeling simulations. Together, these two programs carry out the iterative processes used to implement the model (Fig. 9). These two programs utilize two fundamental files that describe the geometry of a bone cross-section: "outer.txt," which contains a list of points defining the periosteal contour of the bone cross-section, and "inner.txt," which contains a list of points defining the endosteal contour of the bone cross-section. Modifications to the geometry are made by the custom bone modeling program during each time step.

At the beginning of a given simulation time step, VA-Twist reads the two files specifying the sectional geometry and produces a finite element mesh containing 1,080 nodes and 960 elements. Using this mesh VA-Twist computes the sectional properties (cross-sectional area, centroid, second area moments of inertia, and product of inertia) of the cross-section and solves a linear finite element problem to obtain the normalized shear stresses throughout the cross-section due to a unit torsional load. The sectional properties and shear stresses are saved in external files that are subsequently used by the bone modeling program.

After VA-Twist completes its computations, the bone modeling program reads the VA-Twist output files specifying the geometry, sectional properties, and torsional shear stresses. The program computes the magnitudes of applied far-field loads based on the simulated age of the organism. Any number of axial forces directed along the bone's long axis, bending moments, and torques can be applied. Applied axial loads and bending moments are used along with the sectional properties to compute normal stresses based on engineering beam theory (Crandall and Dahl 1959), and the shear stresses are calculated using the torque magnitudes along with the normalized shear stresses calculated by VA-Twist. The effective energy stress at each point on the endosteal and periosteal surfaces is calculated using Eq. (1), and the corresponding daily stress stimulus is calculated using Eq. (2) along with the user-specified number of daily loading cycles. Then, using the intracortical modeling relationship (Fig. 4), the local modeling rates ($\dot{r}_e$ and $\dot{r}_p$) are determined at each point on the endosteal and periosteal contours.

In order to simulate the effects of the adjacent dorsiflexor and plantar flexor muscle groups, periosteal surface pressures were defined along the anterolateral and posterolateral portions of the outer contour using quadratic distributions (Fig. 9b). Using these distributions along with the user-specified daily time of active muscle contraction, the bone modeling program calculated the local surface modeling stimulus. Then, using the daily stress stimulus and the surface modeling stimulus along with the relationship illustrated in Fig. 6, the local modeling rate was obtained at each periosteal and endosteal location.

Based on the local modeling rate and the temporal length of the simulation time step, the locations of all points on the bone surfaces were moved the appropriate distance in a direction normal to the bone surface. In order to simulate bone apposition, points were moved away from the bone surface in the direction of the local outward surface normal. In order to simulate bone resorption, points were moved away from the bone surface in the direction of the local inward surface

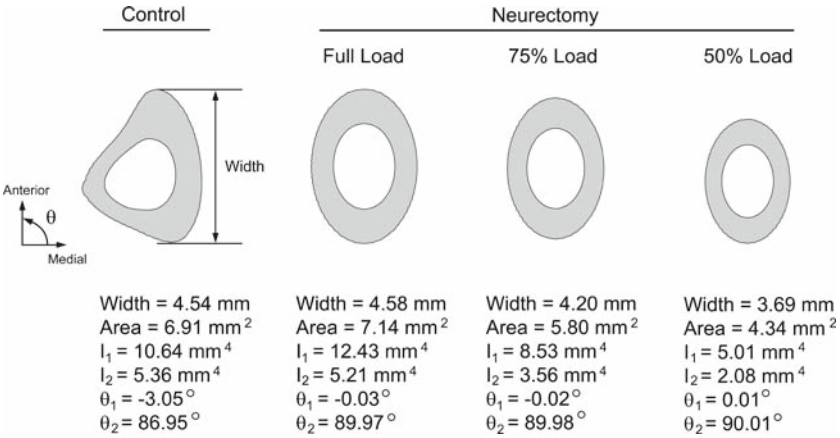

Fig. 12 Cross-sections of the rat tibia at a simulated age of 17 months. Section width is measured in the anterior–posterior direction, and principal angles are measured as indicated on the axes in the lower left corner. Note that the far-field bending moment was applied about the medial-lateral axis ($\theta = 0°$)

normal. The new periosteal and endosteal contours were then saved in updated versions of "outer.txt" and "inner.txt," and the next simulation time step began. The geometries of the inner and outer contours and the local modeling rates were saved after each simulated month in order to track changes in geometry and modeling rates over time. The width of the tibia in the anterior–posterior direction, cross-sectional area, principal moments of inertia (I_1 and I_2), and corresponding principal directions (θ_1 and θ_2) was also recorded after each week of growth.

2.2.2 Model specifics

Initial bone cross-sectional geometry and material properties were chosen in order to approximate the configuration that exists at the beginning of tibial ossification in rats. All simulations began with a circular bone cross-section that had an inner radius of 0.38 mm and an outer radius of 0.40 mm. This cross-section represented the primary bone collar that forms around the midshaft of the rat tibia approximately 6 days before birth (Donaldson 1924). Cross-sections were assumed to be composed entirely of cortical bone with a longitudinal elastic modulus of 17 GPa and a shear modulus of 3.28 GPa, and these material properties were used throughout the duration of the simulations (Reilly and Burstein 1975).

A far-field bending moment and torque were applied for a total of 10,000 loading cycles per day, and a value of m = 4 was used in Eq. (2) in order to calculate the value of Ψ at each point on the periosteal and endosteal contours. The bending moment was applied about the medial-lateral axis and caused compressive stresses within the caudal/posterior aspect of the bone section and tensile stresses within the cranial/anterior aspect of the bone section. The torque was applied about the centroid of the bone section. Both loads were scaled directly with the body weight (BW) of a growing rat in order to simulate the increasing loads that result during growth as a result of increasing muscle size and muscle moment arms (Donaldson 1924; van der Meulen et al. 1993). Scaling factors were chosen in order to produce an overall cross-sectional size at an age of 17 months of approximately 3 mm × 4.5 mm, which was the tibial size measured in a group of mature, normal rats (Kay and Condon 1987). Using this criterion, scaling factors of 5.10 for torque and 7.14 for bending moment were used to produce an applied torque of $T = (5.10 \times \mathrm{BW})$ N·mm and an applied bending moment of $\mathrm{M} = (7.14 \times \mathrm{BW})$ N·mm (Fig. 10).

Periosteal surface pressures due to active muscle contractions were applied to the anterolateral and posterolateral surfaces of the periosteum using quadratic distributions, each of which had a pressure of 0 kPa at the edges and a peak magnitude of 30 kPa at the center (Fig. 9). The pressure distribution on the anterolateral surface simulated the effects of the bulging bellies of the tibialis anterior and extensor hallucis longus muscles, whereas the pressure distribution on the posterolateral surface simulated the effects of the bulging belly of the tibialis posterior muscle. This peak pressure magnitude corresponds to the lower end of the range of pressures measured by Teng and Herring (1998), who implanted pressure transducers between contracting muscles and bone surfaces of the porcine jaw. The two muscle groups were each assumed to contract for a total of 10,000 s per day. Thus the total surface modeling stimulus at the location of the peak pressure was

$$\Psi_s = \frac{(-30\mathrm{kPa}) \times (10,000\,\mathrm{s/day})}{86,400\,\mathrm{s}} = -3.47\mathrm{kPa/day}. \quad (6)$$

Because no data are currently available on the scaling of periosteal surface pressures with age, the peak surface pressure of −30 kPa was maintained throughout the simulation. To maintain the spatial arrangement of the simulated muscles, the total number of surface nodes experiencing periosteal pressure was kept constant (37 nodes for the tibialis anterior and extensor hallucis longus; 31 nodes for the tibialis posterior). The movement of the nodes was controlled solely by the local apposition or resorption rate computed in each simulation step. Therefore the total area of pressure

application was allowed to change along with concurrent changes in size and shape.

To simulate the last 6 gestational days and first 28 days of tibial development, the initial geometry was subjected to the bending moment, torque, and periosteal pressure distributions. At an age of 28 days, the geometry was saved and used as a starting point for four different simulations: a control simulation, a full-load neurectomy simulation, a 75% load neurectomy simulation, and a 50% load neurectomy simulation. In the control simulation, which corresponded to the normally functioning limb in Lanyon's experiment, all far-field loads and periosteal pressures were applied at their normal levels throughout the next 16 months of growth. In the full-load neurectomy simulation, the periosteal surface pressure distributions were removed in order to simulate the effect of sciatic neurectomy, but the far-field loads were maintained at their normal levels. Because no nerve impulses reach the shank muscles in the case of a sciatic neurectomy, the musculature adjacent to the tibia would not be expected to exert significant levels of periosteal surface pressure. However, it is unclear how the far-field loads changed in the hindlimbs of the neurectomized rats in Lanyon's experiment. Thus the far-field load magnitudes were maintained in the full-load neurectomy simulation, and the 75 and 50% load neurectomy simulations were performed in order to determine the effect of far-field load magnitude on tibial development after sciatic neurectomy. In the 75% load simulation, the bending moment and torque magnitudes were 75% of those used in the control and full-load neurectomy simulations, and the magnitudes used in the 50% load simulation were 50% of those used in the control and full-load neurectomy simulations. A time step of 1 day was used in all cases, and the number of daily loading cycles was maintained at 10,000 cycles per day throughout the simulations.

3 Results

From the start of the simulation to an age of 1 week, active bone formation took place at all points on the endosteal and periosteal surfaces (Fig. 11). By an age of two weeks, bone resorption began to occur on the medial side of the endosteal surface, while bone apposition continued at all other locations. This pattern remained up to an age of 4 weeks. Then, once the loading patterns were changed for the neurectomy simulation, the modeling patterns and geometries for the control tibia and neurectomized tibia began to diverge.

In the control tibia, the medial resorption and lateral apposition pattern on the endosteal surface continued throughout the remaining simulation, but the periosteal pattern changed at an age of approximately 5 months. After 5 months of growth, bone resorption began to occur in the regions experiencing periosteal surface pressures, and this pattern continued for the remaining simulation. At an age of 17 months, the control tibia had a distinctly triangular cross-sectional morphology with a slightly concave anterolateral face and a flattened posterolateral face.

In the neurectomy simulations, removal of the periosteal surface pressures produced changes in both the endosteal and periosteal apposition/resorption patterns. By an age of 6 weeks, bone resorption began to occur on the entire endosteal surface, while bone apposition continued on the periosteal surface. This pattern continued throughout the remaining simulation. By an age of 2 months, the tibia obtained a nearly elliptical cross-sectional shape. Periosteal apposition and endosteal resorption produced a smooth, elliptical final geometry at an age of 17 months.

All neurectomy simulations produced similar elliptical cross-sections, and decreased load magnitudes resulted in smaller overall geometries and sectional properties (Fig. 12). The full-load neurectomy simulation resulted in a slight increase in width, cross-sectional area, and maximum moment of inertia (I_1) as compared to the control case, whereas decreases in far-field load magnitudes resulted in decreased sectional properties. The principal direction (θ_1) corresponding to I_1 corresponded very closely to the direction ($\theta = 0°$) of the applied bending moment for the neurectomized tibiae, while the θ_1 for the control tibia was offset from the bending orientation by approximately $-3°$.

4 Discussion

The results of the simulations suggest that bone cross-sectional size is largely determined by the magnitudes of far-field loads and that bone cross-sectional shape is strongly affected by local periosteal surface loads. In the full-load neurectomy simulation, the removal of periosteal pressures at an age of 4 weeks resulted in a 17-month geometry very different from that in the control case, and the differences in shape closely resemble those that occurred in Lanyon's experimental study. The overall sizes of the final control and full-load neurectomy bone sections were very similar: their widths only differed by 0.9% and their cross-sectional areas only differed by 3.3%. However, decreases in far-field load magnitudes resulted in much greater differences in size. In the 75% loading case, the width was 7.5% smaller than that of the control, and the cross-sectional area was 16.1% smaller than that of the control. In the 50% loading case, the width was 18.7% smaller than that of the control, and the cross-sectional area was 37.2% smaller than that of the control. Thus the magnitudes of the far-field loads dictated cross-sectional size, and this was due to the relationship between the daily stress stimulus and modeling rate. Recall that, in Lanyon's experiment, the tibiae from the neurectomized limbs attained an average width approximately 11% less than

that of the functioning limbs. The simulation results suggest that the daily stress stimulus due to far-field loading in Lanyon's neurectomized rats was between 50 and 75% of that in the normal rats.

The daily stress stimulus modeling framework produces a cross-sectional structure that is well-suited for supporting far-field loads. Bone is added where intracortical stresses are high and removed where intracortical stresses are low. Because the daily stress stimulus modeling approach aims to maintain bone stresses within the range of the "lazy zone," increases in periosteal stresses will lead to increased rates of bone formation on the periosteum and subsequent increases in bone size. Similarly, decreased levels of loading result in lower formation rates or even bone resorption, leading to a smaller cross-sectional size. The periosteal response to loads applied perpendicular to the bone surface presumably operates through a separate stimulus-response process and therefore has the ability to modify the local modeling rate induced by the far-field loads. The result is a mechaniobiological system in which cross-sectional size is determined by large-scale mechanical demands, while local cross-sectional shape is largely determined by the relatively smaller loads imposed by adjacent structures.

The simulations also suggest that loads applied directly to the periosteal surface may indirectly affect the bone modeling response on the endosteal surface. The periosteal surface pressures applied in the control simulation caused a reduction in periosteal bone apposition rate and, after 5 months of growth, periosteal resorption. These effects led to local cortical thinning and increased intracortical stresses, which subsequently led to an appositional response on the adjacent endosteal surface. In the converse case, periosteal bone apposition leads to cortical thickening, decreased intracortical stresses, and endosteal resorption. The result is the pattern seen in the control tibia in Fig. 11: regions of endosteal bone apposition adjacent to regions of periosteal resorption, and vice versa. It may seem counterintuitive that endosteal modeling rates would be affected by relatively small loads on the periosteal surface, but the results suggest that changes in intracortical stresses due to local periosteal modeling can lead to an indirect coupling between periosteal loading and endosteal modeling. This interaction may explain the patterns seen in tetracycline studies of growing bones. In a tetracycline study of the normal, growing rat tibia, Yeh et al. (1993) observed endosteal bone apposition in areas adjacent to regions of periosteal resorption, and vice versa. The "modeling drifts" that occur during the growth of the rat ulna also demonstrate this relationship (Mosley and Lanyon 1998).

The difference between the orientation of the applied bending moment and the direction θ_1 in the control simulation also has implications in understanding bone morphogenesis. Because the periosteal pressures in our simulations resulted in asymmetric changes in bone morphology, the direction of the bone's maximum bending stiffness did not correspond exactly with the direction of the applied bending moment. Thus the influence of periosteal surface loads on bone geometry may explain why some bones do not develop maximum flexural stiffness to resist bending in directions corresponding to in vivo surface strain measurements. In studies of the canine radius and ovine tibia, surface strain gage measurements obtained during walking and treadmill running revealed that these bones habitually experienced bending loads in a direction near to that of the *minimum* bending stiffness (Carter et al. 1981; Lieberman et al. 2004). These findings have led some researchers to question the validity of the concept that bone morphology reflects bone function (Pearson and Lieberman 2004; Ruff et al. 2006). However, our simulation of rat tibia development suggests that periosteal surface loads can affect the direction of a bone's maximum bending stiffness.

Although our simulation produced a maximum bending stiffness offset by only 3° from the direction of the applied bending load, other anatomic configurations may produce much greater discrepancies. If sufficient levels of periosteal surface pressure are applied to two opposing periosteal surfaces, we hypothesize that the mechanobiological effects of these pressures would prevent the bone apposition needed to align the direction of maximum bending stiffness with the direction of the applied bending moment (Fig. 13). In this case the effects of periosteal surface pressures would produce a bone shape that has a direction of *minimum* bending stiffness aligned with the applied bending moment. In short, bones do not always obtain an optimal cross-sectional geometry for resisting applied far-field loads. Instead, the interaction between the responses to intracortical stresses and periosteal surface loads leads to a "compromise" between the drive towards optimal mechanical support and the need to accommodate adjacent structures.

Initial skeletal patterning occurs under the direction of positional information controlled by cell-to-cell communication and the influence of diffusible signaling molecules. These biological signals may work in combination with periosteal loads to produce the similarities in bone cross-sectional shape that exist across a wide variety of species. Locomotor posture and muscle moment arms change as a function of animal size, affecting the stress distribution within bones and bone cross-sectional size (Biewener 1991; Carter and Beaupré 2001). As a result bone strains during vigorous activities remain relatively constant across a wide range of animal sizes (Rubin and Lanyon 1984). This suggests that the mechanobiological response to intracortical stresses and strains has been conserved through terrestrial vertebrate evolution, leading to scaling in bone size with body mass while maintaining a relatively constant bone diameter to cortical thickness ratio (Currey and Alexander 1985). Differences in gait and locomotor posture would be expected to lead

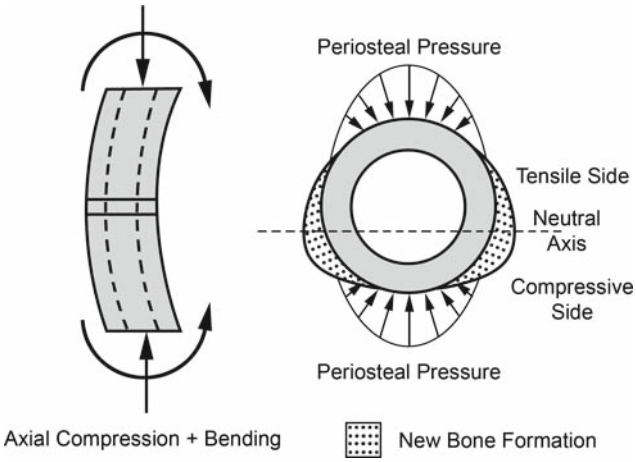

Fig. 13 Hypothesized effects of diametrically opposed periosteal pressure distributions on bone cross-sectional growth. *Left* Bending moment and axial compression applied to a tubular long bone. The section of interest is indicated at the mid-diaphysis. *Right* Axial view of the section of interest. Intracortical stresses due to axial compression and bending produce the highest strains at locations furthest from the neutral axis. Because of the superimposed axial compression, intracortical stresses on the compressive side are higher than those on the tensile side. Periosteal pressures prevent bone formation, limiting new bone formation to regions near the neutral axis, where stresses are relatively low. The resulting bone cross-section has a minimum bending stiffness closely corresponding to the direction in which it is habitually bent

to very different spatial strain distribution patterns between different species, especially between bipedal and quadrupedal animals. Given the similarities in bone modeling response to intracortical stresses, differences in spatial strain distribution would be expected to produce large variations in cross-sectional shape. However, the similar anatomical arrangement of muscle bellies, muscle attachments, and other structures surrounding bone surfaces that arises during initial patterning may produce periosteal loading effects that lead to similarities in bone shape (Fig. 1). Early development of avian bones is also affected by periosteal pressures and tensile strains (Amprino 1985), suggesting that the general periosteal loading/modeling relationships may extend to an even wider variety of vertebrate species.

While the focus of this study was on the effects of periosteal surface pressures on the tibia, there are certainly other mechanobiological factors that may contribute to the development of bone cross-sectional geometry. The tensile strains that exist at tendon insertions likely affect intracortical stress patterns through their strong connections to bone through Sharpey's fibers, and periosteal tension may simultaneously occur at sites adjacent to tendon insertions. These tensile strains, which occur as a result of skeletal muscle contractions, may work in concert with growth-generated tensile strains in guiding the development of bony ridges (Hamburger and Waugh 1940; Henderson and Carter 2002). Transcortical pressure gradients may also affect bone surface modeling rates through the effects of fluid flow through the bone matrix and pressurization of the periosteum (Qin et al. 2003; Wang et al. 2003). In addition to directly deforming cells and possibly affecting the local blood supply, applied periosteal pressures and tensile strains would also be expected to affect transcortical pressure gradients. The effects of periosteal surface loads on surface modeling rates may be induced by this stimulus. The rotational shifting of the intracortical stress distribution during gait and other physical activities may also affect bone development and functional adaptation (Levenston et al. 1998; Peterman et al. 2001). All of these factors may act along with the periosteal loading environment to produce local variations in bone cross-sectional shapes.

A number of assumptions and simplifications were applied in the development of the models used in this study. The bone cross-sections were assumed to consist entirely of transversely isotropic cortical bone. In reality there is variation in bone density within different bone sections, and this will affect the sectional properties and direction of maximum stiffness. The model also assumes that there is an instantaneous modeling response with no coupling between osteoclastic and osteoblastic activity. In reality there is a time lag between loading incidents and the local bone modeling response, and evidence suggests that there is an interaction between osteoclastic and osteoblastic activities (Roberts and Chase 1981; King et al. 1991; Martin and Ng 1994; Boppart et al. 1998; Cullen et al. 2000). The model also assumes that bone responds in an identical fashion to intracortical tensile stress and compressive stress. Evidence suggests that bones that experience bending loads may in fact exhibit different modeling responses in areas of longitudinal tension as opposed to longitudinal compression (Lanyon and Baggott 1976; Skedros et al. 2004; Kotha et al. 2004). Future models that take into account the difference between compressive and tensile stresses can be implemented by developing separate rate modeling curves for intracortical compression and tension.

Both the far-field loads and periosteal pressure distributions applied in the simulations were much simpler than the in vivo loading environment that exists during a rat's day-to-day activities. However, the combination of bending and torsion possibly captures the dominant far-field loading modes, and the periosteal pressure magnitudes were within the range measured in experiments (Teng and Herring 1998). The choice to apply 10,000 load cycles per day was based upon past simulations performed in our laboratory (van der Meulen et al. 1993; Levenston et al. 1998). The load magnitude used in the control and full-load neurectomy simulations was scaled to produce a final cross-sectional size similar to that measured in a group of normal, mature rats (Kay and Condon 1987). Alternatively, fewer loading cycles with a higher magnitude of applied stress can be used to

achieve the same daily stress stimulus using Eq. (2). The loads also did not include any shift in direction, which has been shown to occur in the human tibia during in vivo measurements and in vitro gait simulations (Lanyon et al. 1975; Peterman et al. 2001). A shift in loading direction, as opposed to just a change in load magnitude, would also likely occur in the event of a sciatic neurectomy in rats. However, with no information on the direction of the in vivo loads that occurred in the rat experiment performed by Lanyon (1980), we chose only to explore the resulting changes in load magnitude and periosteal pressure relief. The loss of normal muscle function in Lanyon's study possibly led to changes in the far-field load directions, and it is possible that the observed differences in cross-sectional shape occurred due to resultant changes in intracortical strain distribution. The peak periosteal pressure magnitudes used in the control simulations also remained unchanged throughout the lifetime of the rat, and no areas of tensile strain perpendicular to the periosteal surface were included in the analysis. It is likely that the pressures change over time as the bone surface accommodates the adjacent musculature, and tensile strains applied at tendon insertions may also have important effects on bone morphogenesis. As researchers continue to study bone's response to different types of loads, it is likely that more specific information on the types and directions of applied loads will be made available for use in models such as the one presented here. Despite the simplifications that were necessary in order to implement the models used in this study, the simulations produced tibial cross-sections with sizes and shapes similar to those seen in experiments. Therefore the results of this study suggest that this model captures the most important elements of the system.

Although the model used in this study provides a phenomenological description of the effects of periosteal surface loads, further studies are needed to elucidate the cellular and biochemical processes through which these mechanical signals are translated in to a bone modeling response. Experiments in which different levels of compressive loads are applied to the periosteum would help to quantify the relationship between pressure and periosteal blood supply and the resulting effects on the osteoblasts and osteoblast precursors in the cambium layer. Cell culture experiments similar to those performed by Kanzaki et al. (2002) could be used to determine the level of applied compression needed to increase osteoclastogenesis in periosteal cells. Together, these two sets of experiments would help to determine the specific biological mechanisms that produce bone modeling effects with impeded blood flow and direct cellular deformation. Further experiments on periosteal distraction osteogenesis (Schmidt et al. 2002) and the effects of tensile strain on periosteal cells (Kanno et al. 2005) would help to quantify and explain the bone modeling that occurs in response to periosteal tension.

The bone modeling simulations performed in this study provide a mechanobiological explanation of the similarities in tibial morphology seen across a wide variety of species. Periosteal surface loads may be an important component of a group of mechanical stimuli, including intracortical stresses and transcortical pressure gradients, that influence the development of bone cross-sectional shapes. Bone development and adaptation are achieved via biological processes. However, the local mechanical environment resulting from the spatial arrangement of bones and musculature is possibly an important mechanobiological stimulus. As shown by this study, the development of the triangular cross-sectional shape in terrestrial mammals may in fact depend on the mechanobiological relationship between muscle function and local bone modeling rates. These models, along with the previously discussed experiments of Ráliš et al. (1976) and Lanyon (1980), suggest that normal muscle function plays an important role in the development of the triangular cross-sectional morphology of the tibial diaphysis. In concert with Cuvier's concept of a correlation of parts and Lanyon's hypothesis of bone accommodation, the results of this study suggest that anatomic structures located adjacent to bones are important in determining skeletal morphology.

Acknowledgments The authors would like to thank Gary Beaupré, Jay Henderson, Emily Clowes, Julia Chen, and Betty Zhao for their input and assistance in developing the mechanobiological modeling framework presented in this paper, and Thomas Lang and John Hutchinson for providing the images of large mammal bones. This work was funded by the United States Department of Veterans Affairs Merit Review grant A2723R and a Stanford University Office of Technology Licensing Fellowship.

References

Agur AMR, Lee MJ (1999) Grant's Atlas of anatomy, 10th edn. Lippincott Williams and Wilkins, Philadelphia

Amprino R (1985) The influence of stress and strain in the early development of shaft bones. An experimental study on the chick embryo tibia. Anat Embryol (Berl) 172:49–60

Arnett TR, Gibbons DC, Utting JC, Orris IR, Hoebertz A, Rosendaal M, Meghji S (2003) Hypoxia is a major stimulator of osteoclast formation and bone resorption. J Cell Physiol 196:2–8

Beaupré GS, Orr TE, Carter DR (1990a) An approach for time-dependent bone modeling and remodeling–theoretical development. J Orthop Res 8:651–661

Beaupré GS, Orr TE, Carter DR (1990b) An approach for time-dependent bone modeling and remodeling-application: a preliminary remodeling simulation. J Orthop Res 8:662–670

Biewener AA (1991) Musculoskeletal size in relation to body size. J Biomech 24 (Suppl) 1:19–29

Boppart MD, Kimmel DB, Yee JA, Cullen DM (1998) Time course of osteoblast appearance after in vivo mechanical loading. Bone 23:409–415

Carter DR, Beaupré GS (2001) Skeletal function and form: mechanobiology of skeletal development, aging, and regeneration. Cambridge University Press, Cambridge, UK

Carter DR, Fyhrie DP, Whalen RT (1987) Trabecular bone density and loading history: regulation of connective tissue biology by mechanical energy. J Biomech 20:785–794
Carter DR, Harris WH, Vasu R, Caler WE (1981) The mechanical and biological response of cortical bone to in vivo strain histories. In: Mechanical properties of bone-AMD, Vol. 45. The American Society of Mechanical Engineers, New York, pp 81–92
Cowin SC (1984) Mechanical modeling of the stress adaptation process in bone. Calcif Tissue Int 36:S98–S103
Cowin SC, Hart RT, Balser JR, Kohn DH (1985) Functional adaptation in long bones: establishing in vivo values for surface remodeling rate coefficients. J Biomech 18:665–684
Crandall SH, Dahl NC (1959) An introduction to the mechanics of solids. McGraw-Hill, New York
Cullen DM, Smith RT, Akhter MP (2000) Time course for bone formation with long-term external mechanical loading. J Appl Physiol 88:1943–1948
Currey JD, Alexander RM (1985) The thickness of the walls of tubular bones. J Zool Lond 206:453–468
Donaldson HH (1924) The rat: data and reference tables for the albino rat (Mus norvegius albinus) and the Norway rat (Mus norvegius), Philadelphia
Ek AC, Gustavsson G, Lewis DH (1987) Skin blood flow in relation to external pressure and temperature in the supine position on a standard hospital mattress. Scand J Rehabil Med 19:121–126
Evans HE, Christensen GC (1979) Miller's anatomy of the dog. Saunders, Philadelphia
Feik SA, Storey E, Ellender G (1987) Stress induced periosteal changes. Br J Exp Pathol 68:803–813
Fong KD, Nacamuli RP, Loboa EG, Henderson JH, Fang TD, Song HM, Cowan CM, Warren SM, Carter DR, Longaker MT (2003) Equibiaxial tensile strain affects calvarial osteoblast biology. J Craniofac Surg 14:348–355
Fyhrie DP, Carter DR (1986) A unifying principle relating stress to trabecular bone morphology. J Orthop Res 4:304–317
Gooding CA, Glickman MG, Suydam MJ (1969) Fate of rib notching after correction of aortic coarctation. Am J Roentgenol Radium Ther Nucl Med 106:21–23
Hall RF Jr., Watt DH (1986) Osseous changes due to a false aneurysm of the proper digital artery: a case report. J Hand Surg [Am] 11:440–442
Hamburger V, Waugh M (1940) The primary development of the skeleton in nerveless and poorly innervated limb transplants of chick embryos. Physiol Zool 13:367–384
Hart RT, Davy DT, Heiple KG (1984) Mathematical modeling and numerical solutions for functionally dependent bone modeling. Calcif Tissue Int 36:S104–S109
Henderson JH, Carter DR (2002) Mechanical induction in limb morphogenesis: the role of growth-generated strains and pressures. Bone 31:645–653
Henderson JH, Longaker MT, Carter DR (2004) Sutural bone deposition rate and strain magnitude during cranial development. Bone 34:271–280
Huiskes R, Weinans H, Grootenboer HJ, Dalstra M, Fudala B, Slooff TJ (1987) Adaptive bone-remodeling theory applied to prosthetic-design analysis. J Biomech 20:1135–1150
Ikegame M, Ishibashi O, Yoshizawa T, Shimomura J, Komori T, Ozawa H, Kawashima H (2001) Tensile stress induces bone morphogenic protein 4 in preosteoblastic and fibroblastic cells, which later differentiate into osteoblasts leading to osteogenesis in the mouse calvariae in organ culture. J Bone Miner Res 16:24–32
Iwasaki LR, Crouch LD, Reinhardt RA, Nickel JC (2004) The velocity of human orthodontic tooth movement is related to stress magnitude, growth status, and the ratio of cytokines in gingival crevicular fluid. In: Biological mechanisms of tooth movement and craniofacial adaptation. Harvard Society for the Advancement of Orthodontics, Boston
Jaworski ZF, Liskova-Kiar M, Uhthoff HK (1980) Effect of long-term immobilisation on the pattern of bone loss in older dogs. J Bone Joint Surg Br 62-B:104–110
Jepsen KJ, Davy DT (1997) Comparison of damage accumulation measures in human cortical bone. J Biomech 30:891–894
Kaneko TS, Pejcic MR, Tehranzadeh J, Keyak JH (2003) Relationships between material properties and CT scan data of cortical bone with and without metastatic lesions. Med Eng Phys 25:445–454
Kanno T, Takahashi T, Ariyoshi W, Haga M, Nishihara T (2005) Tensile mechanical strain up-regulates Runx2 and osteogenic factor expression in human periosteal cells: implications for distraction osteogenesis. J Oral Maxillofac Surg 63:499–504
Kanzaki H, Chiba M, Shimizu Y, Mitani H (2002) Periodontal ligament cells under mechanical stress induce osteoclastogenesis by receptor activator of nuclear factor kappaB ligand up-regulation via prostaglandin E2 synthesis. J Bone Miner Res 17:210–220
Kay ED, Condon K (1987) Skeletal changes in the hindlimbs of bipedal rats. Anat Rec 218:1–4
King GJ, Keeling SD, Wronski TJ (1991) Histomorphometric study of alveolar bone turnover in orthodontic tooth movement. Bone 12:401–409
Kotha SP, Hsieh YF, Strigel RM, Muller R, Silva MJ (2004) Experimental and finite element analysis of the rat ulnar loading model-correlations between strain and bone formation following fatigue loading. J Biomech 37:541–548
Lanyon LE (1980) The influence of function on the development of bone curvature. An experimental study on the rat tibia. J Zool 192:457–466
Lanyon LE, Baggott DG (1976) Mechanical function as an influence on the structure and form of bone. J Bone Joint Surg Br 58-B: 436–443
Lanyon LE, Hampson WG, Goodship AE, Shah JS (1975) Bone deformation recorded in vivo from strain gages attached to the human tibial shaft. Acta Orthop Scand 46:256–268
Levenston ME, Beaupré GS, Carter DR (1998) Loading mode interactions in simulations of long bone cross-sectional adaptation. Comput Methods Biomech Biomed Eng 1:303–319
Lieberman DE, Polk JD, Demes B (2004) Predicting long bone loading from cross-sectional geometry. Am J Phys Anthropol 123:156–171
Loboa EG, Fang TD, Warren SM, Lindsey DP, Fong KD, Longaker MT, Carter DR (2004) Mechanobiology of mandibular distraction osteogenesis:experimental analyses with a rat model. Bone 34:336–343
Martens M, Van Audekercke R, De Meester P, Mulier JC (1981) The geometrical properties of human femur and tibia and their importance for the mechanical behaviour of these bone structures. Arch Orthop Trauma Surg 98:113–120
Martin TJ, Ng KW (1994) Mechanisms by which cells of the osteoblast lineage control osteoclast formation and activity. J Cell Biochem 56:357–366
McClure RC, Dallman MJ, Garrett PD (1973) Anatomy of the cat: an atlas, text, and dissection guide. Lea and Febiger, Philadelphia
Mikic B, Carter DR (1995) Bone strain gage data and theoretical models of functional adaptation. J Biomech 28:465–469
Mosley JR, Lanyon LE (1998) Strain rate as a controlling influence on adaptive modeling in response to dynamic loading of the ulna in growing male rats. Bone 23:313–318
Orisek BS, Chole RA (1987) Pressures exerted by experimental cholesteatomas. Arch Otolaryngol Head Neck Surg 113:386–391
Pearson OM, Lieberman DE (2004) The aging of Wolff's "law": ontogeny and responses to mechanical loading in cortical bone. Am J Phys Anthropol Suppl 39:63–99

Peterman MM, Hamel AJ, Cavanagh PR, Piazza SJ, Sharkey NA (2001) In vitro modeling of human tibial strains during exercise in microgravity. J Biomech 34:693–698

Qin Y-X, Kaplan T, Saldanha A, Rubin C (2003) Fluid pressure gradients, arising from oscillations in intramedullary pressure, is correlated with the formation of bone and inhibition of intracortical porosity. J Biomech 36:1427–1437

Ráliš ZA, Ráliš HM, Randall M, Watkins G, Blake PD (1976) Changes in shape, ossification and quality of bones in children with spina bifida. Dev Med Child Neurol Suppl:29–41

Reilly DT, Burstein AH (1975) The elastic and ultimate properties of compact bone tissue. J Biomech 8:393–405

Roberts WE, Chase DC (1981) Kinetics of cell proliferation and migration associated with orthodontically-induced osteogenesis. J Dent Res 60:174–181

Rubin CT, Lanyon LE (1984) Dynamic strain similarity in vertebrates; an alternative to allometric limb bone scaling. J Theor Biol 107:321–327

Rudwick MJS (1997) Georges Cuvier, fossil bones, and geological catastrophes. The University of Chicago Press, Chicago

Ruff CB, Holt B, Trinkaus E (2006) Who's afraid of the big bad Wolff? "Wolff's law" and bone functional adaptation. Am J Phys Anthropol 129:484–498

Ruff CB, Hayes WC (1982) Subperiosteal expansion and cortical remodeling of the human femur and tibia with aging. Science 217:945–948

Salim A, Nacamuli RP, Morgan EF, Giaccia AJ, Longaker MT (2004) Transient changes in oxygen tension inhibit osteogenic differentiation and Runx2 expression in osteoblasts. J Biol Chem 279:40007–40016

Sato T, Hara T, Mori S, Shirai H, Minagi S (1998) Threshold for bone resorption induced by continuous and intermittent pressure in the rat hard palate. J Dent Res 77:387–392

Schmidt BL, Kung L, Jones C, Casap N (2002) Induced osteogenesis by periosteal distraction. J Oral Maxillofac Surg 60:1170–1175

Skedros JG, Hunt KJ, Bloebaum RD (2004) Relationships of loading history and structural and material characteristics of bone:development of the mule deer calcaneous. J Morphol 259:281–307

Skripitz R, Aspenberg P (2000) Pressure-induced periprosthetic osteolysis: a rat model. J Orthop Res 18:481–484

Sikes SK (1971) The Natural History of the African Elephant. American Elsevier Publishing Company, Inc., New York

Sontag W (1992) Age-dependent morphometric alterations in the distal femora of male and female rats. Bone 13:297–310

Teng S, Herring SW (1998) Compressive loading on bone surfaces from muscular contraction: an in vivo study in the miniature pig, Sus scrofa. J Morphol 238:71–80

van der Meulen MCH, Beaupré GS, Carter DR (1993) Mechanobiologic influences in long bone cross-sectional growth. Bone 14:635–642

von Böhl M, Maltha JC, Von Den Hoff JW, Kuijpers-Jagtman AM (2004) Focal hyalinization during experimental tooth movement in beagle dogs. Am J Orthod Dentofacial Orthop 125:615–623

Voyvodic F, Sage MR, Brophy BP (1992) Intracerebral ganglioglioma. Australas Radiol 36:153–154

Wang K, Hodges M (1994) Images in cardiovascular medicine. Erosion of lumbar vertebral bodies due to abdominal aortic aneurysm. Circulation 89:1317

Wang L, Fritton SP, Weinbaum S, Cowin SC (2003) On bone adaptation due to venous stasis. J Biomech 36:1439–1451

Yeh JK, Liu CC, Aloia JF (1993) Effects of exercise and immobilization on bone formation and resorption in young rats. Am J Physiol 264(2 Pt 1):E182–9

Yochum TR, Rowe LJ (2005) Yochum and Rowe's essentials of skeletal radiology, 3rd edn. Lippincott Williams and Wilkins, Baltimore